Virtual Spring–Damping System for Flow-Induced Motion Experiments

Hai Sun[1]
Assistant Professor
Harbin Engineering University,
Harbin 150001, China;
Department Naval Architecture
and Marine Engineering,
University of Michigan,
Ann Arbor, MI 48109-2145
e-mail: hais@umich.edu

Eun Soo Kim[1]
Department Naval Architecture
and Marine Engineering,
University of Michigan,
Ann Arbor, Michigan 48109-2145
e-mail: bblwith@umich.edu

Marinos P. Bernitsas
Vortex Hydro Energy Inc.,
Ann Arbor, MI 48108
e-mail: marinosbern@gmail.com

Michael M. Bernitsas[2]
Mortimer E. Cooley Collegiate Professor
of Naval Architecture and Marine Engineering
and Mechanical Engineering,
University of Michigan,
Ann Arbor, MI 48109-2145;
Vortex Hydro Energy Inc.,
Ann Arbor, MI 48108
e-mail: michaelb@umich.edu

Flow-induced motion (FIM) experiments of a single circular cylinder or multiple cylinders in an array involve several configuration and hydrodynamic parameters, such as diameter, mass, damping, stiffness, spacing, Reynolds number, and flow regime, and deviation from circular cross section. Due to the importance of the FIM both in suppression for structural robustness and in enhancement for hydrokinetic energy conversion, systematic experiments are being conducted since the early 1960s and several more decades of experimentation are required. Change of springs and dampers is time consuming and requires frequent recalibration. Emulating springs and dampers with a controller makes parameter change efficient and accurate. There are two approaches to this problem: The first involves the hydrodynamic force in the closed-loop and is easier to implement. The second called virtual damping and spring (V_{ck}) does not involve the hydrodynamic force in the closed-loop but requires an elaborate system identification (SI) process. V_{ck} was developed in the Marine Renewable Energy Laboratory (MRELab) of the University of Michigan for the first time in 2009 and resulted in extensive data generation. In this paper, the second generation of V_{ck} is developed and validated by comparison of the FIM experiments between a V_{ck} emulated oscillator and an oscillator with physical springs and dampers. The main findings are: (a) the V_{ck} system developed keeps the hydrodynamic force out of the control-loop and, thus, does not bias the FIM, (b) The controller-induced lag is minimal and significantly reduced compared to the first generation of V_{ck} built in the MRELab due to use of an Arduino embedded board to control a servomotor instead of Labview, (c) The SI process revealed a static, third-order, nonlinear viscous model but no need for dynamic terms with memory, and (d) The agreement between real and virtual springs and dampers is excellent in FIM including vortex-induced vibrations (VIVs) and galloping measurements over the entire range of spring constants and velocities tested ($16{,}000 < Re < 140{,}000$). [DOI: 10.1115/1.4031327]

1 Introduction

FIMs present a source of challenge for diverse structures in steady flows such as heat exchangers, bridges, buildings, offshore structures, or power-transmission cables. The most common FIM phenomenon is vortex-induced vibration (VIV), which was first observed by Leonardo da Vinci in 1504. The first mathematical formulation was done by Strouhal in 1878. Comprehensive reviews of VIV have been published by Bearman [1,2], Sarpkaya [3], and Williamson and Govardhan [4].

Galloping is another form of the FIM. It is an aero/hydro-elastic instability, which is characterized by lower frequencies and larger amplitudes, than the VIV and is perpendicular to the flow [5,6]. It is more vigorous and destructive than the VIV, yet not as complex a phenomenon as VIV. Galloping does not depend on the vortex formation, occurs above a critical flow speed, and has much bigger amplitude of oscillation.

For a single rigid cylinder on elastic supports in a cross-flow, FIM is initiated as VIV due to vortex shedding at low speeds, when the reduced velocity reaches the synchronization range starting with the initial branch. This response amplitude increases with the velocity of the flow in the upper branch. It is followed by the lower branch with smaller response, then the desynchronization zone, and then the end of the VIV synchronization range. The various branches differ significantly depending on whether the flow regime is TrSL2 or TrSL3 [7]. Williamson and Govardhan [4] conducted experiments for Re about 3800 in TrSL2 ($1000 < \mathrm{Re} < 20{,}000$) and response amplitude reached one cylinder diameter. Bernitsas et al. [8] and Raghavan and Bernitsas [9] conducted experiments for $16{,}000 < \mathrm{Re} < 140{,}000$ in the TrSL3 ($20{,}000 < \mathrm{Re} < 300{,}000$) flow regime. In TrSL3, the shear layers on the two sides of the cylinder are saturated and vortex roll-up is stronger resulting in shorter formation length of the von Kármán vortices than in the TrSL2 regime. Thus, when vortices shed they are closer to the after-body of the cylinder resulting in high lift and amplitude response that reaches two diameters.

At higher speeds, galloping may be reached depending on the geometric deviation of the cylinder from the circular cross section [10]. Experimentally, galloping reaches the physical limits of the oscillator in the experimental facility or structural failure [11,12].

Multiple cylinders in a school as in Fig. 1 exhibit the two FIMs described above. In addition, interference effects become very significant [13] resulting in an enhanced VIV or galloping and gap-flow induced instabilities. Specifically, depending on the relative location of cylinders, the flow around the first cylinder may go between the two cylinders resulting in enhanced forces due to Bernoulli Effect and instabilities [14–16].

FIMs are suppressed in engineering applications because of their destructive nature. On the other hand, by enhancing and controlling FIM the Marine Renewable Energy Laboratory (MRELab) at the University of Michigan, developed the VIVACE converter [17–21] to convert marine hydrokinetic (MHK) energy to electricity. The concept is being advanced continually in Ph.D. thesis [12,22–27] and scientific papers. Relevant research on

[1]H. Sun and E. S. Kim contributed equally to this work.
[2]Corresponding author.

Contributed by the Ocean, Offshore, and Arctic Engineering Division of ASME for publication in the Journal of Offshore Mechanics and Arctic Engineering. Manuscript received February 14, 2015; final manuscript received July 19, 2015; published online September 10, 2015. Assoc. Editor: Yi-Hsiang Yu.

harvesting MHK energy using VIVs has been published in several countries: [28] (TX), [29] (Switzerland and France), [30] (Spain), [31] (Greece), and [32] (China).

The research objective of the MRELab is to study the FIMs and find ways to enhance them in order to design multicylinder Vortex Induced Vibration for Aquatic Clean Energy (VIVACE) converters and optimize their power output for a broad range of velocities. Power envelopes as a function of flow speed and type of FIM including need to be generated. FIMs studied in the process include VIVs, galloping, and gap flow. Generating power envelopes in such a large parametric design space and for different FIM phenomena is equivalent to finding the efficiency of propellers with different number of blades and geometric properties. Further, in open-water propeller tests all blades are in equivalent position while in schools of cylinders the hydrodynamics of each cylinder changes depending on the cylinder relative location in the school.

To enable such intense experimentation, a reliable V_{ck} system is developed, built, and validated in this work. The V_{ck} system emulates the mechanical side of the oscillator only using controls without including the hydrodynamic force in the closed-loop to prevent bias and minimize the added phase lag between force and displacement.

Conducting tests with real springs and dampers requires lengthy preparation for each set of experiments. A more efficient way to conduct experiments faster and accurately is developed based in this work on a controller embedded virtual spring–damping system (V_{ck}) that does not include the hydrodynamic force in the closed-loop. Each oscillator consists of one V_{ck}, one interchangeable cylinder moving on submerged roller blocks and driven by the fluid flow, and connected to the controller through belts and pulleys. It is designed to achieve the desired static/dynamic friction through the V_{ck}. An Arduino-embedded board controls a servomotor with an optical encoder, which enables real-time position/speed measurement. A SI methodology is developed making it possible to identify the damping model of any oscillator, which is typically significantly more complicated than the classical linear-viscous model. Upon completion of the SI process for an oscillator, the controller subtracts the nonlinear damping model leaving the system with zero damping. Then, a mathematically linear viscous damping model is added, thus, resulting in a system with real linear-viscous damping. This process enables changing the spring constant and harnessing damping through the controller instantly. Experiments are then conducted with both real spring dampers and V_{ck} to validate the process. All FIM experiments are conducted in the low turbulence free surface water (LTFSW) channel of the University of Michigan at $16{,}000 < \mathrm{Re} < 140{,}000$.

The drawback of this approach is that it requires extensive SI to identify accurately the spring constant and system damping. The former is relatively easy but the identification of the system damping requires extensive testing with multiple different driving functions and velocity ramps [33]. On the other hand, once the damping is identified it can be subtracted to achieve zero damping and then impose any exact function of viscous damping linear or nonlinear.

The alternative method of measuring the hydrodynamic force and solving the differential equation of motion to find and impose the displacement is much faster but keeps the hydrodynamic force in the control loop. That results in 5–12 deg added phase-lag. This method was developed by Smogeli et al. [34] and adopted more recently by Mackowski and Williamson [35].

The development and validation of the V_{ck} system is presented in this paper. In Sec. 2, the system is described. In Sec. 3, the SI process, which is very elaborate and time consuming, is presented in detail. In Sec. 4, tests are conducted with the V_{ck} system and results are compared to experiments with physical springs and dampers for validation.

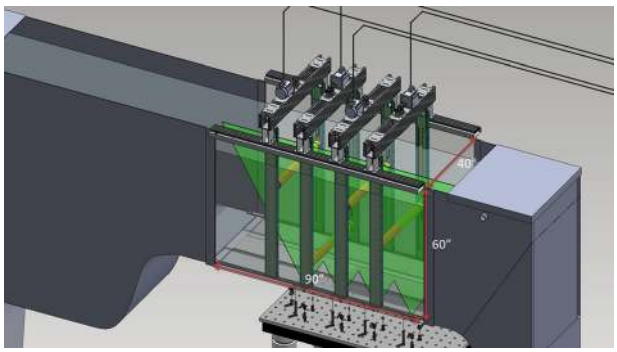

Fig. 1 Design of four VIVACE converters in the new LTFSW channel

2 System Description

In this section, the oscillator is described and modeled mathematically including the V_{ck} system. The SI making possible to realize and implement the V_{ck} system is presented in Sec. 3.

2.1 Oscillator Simulated by the V_{ck} System. The simplest form of the VIVACE converter consists of a single smooth cylinder suspended by springs with a V_{ck} system. Figure 1 shows four such oscillators in an array (school). In early versions of the oscillator in the MRELab, the system was operational on physical springs and dampers. For high-energy conversion, the oscillator needs to have minimal system damping and additional damping for harnessing MHK energy. The total damping cannot exceed certain limit or the FIM—VIV and galloping alike—will be suppressed. If the total damping is above optimal, it will decrease the efficiency of the VIVACE converter. For systematic testing, two issues are important: (a) Changing the physical springs and dampers requires extensive preparation for calibration and alignment and (b) The viscous damping of the system is rarely linear as modeled in classical vibration textbooks. To compensate for these two major challenges, Lee et al. [33] and Lee and Bernitsas [36] introduced and implemented the virtual spring-damping device called V_{ck} system.

V_{ck} is a feedback loop, which uses the servomotor encoder to keep track of the position and velocity of the cylinder and provide the necessary torque to simulate the spring stiffness and provide the linear viscous-damping required. This logic keeps the hydrodynamics out of the control loop making it possible to simulate the mechanical part of the oscillator only, without affecting the hydrodynamic excitation. The V_{ck} end-product provides the experimental setup the flexibility to input the values of spring stiffness and linear viscous damping into the controller and continue the experiments without interruption. This huge advantage comes at the expense of extensive time in V_{ck} system development.

It is critical to compare the accuracy of the V_{ck} system to implement a mechanical oscillator with the desired damping and spring constants. That requires systematic calibration followed by comparison of V_{ck} to an oscillator with physical springs and dampers. The process requires performing repeated experiments in free air and in the LTFSW channel of the MRELab for SI. A nonlinear model for damping is defined after many trials. The resulting damping model is subtracted resulting in a zero damping system. Then, a linear viscous damping model is added producing a perfectly linear viscous damping matching the textbook oscillator models.

The earlier implementation of a virtual system [33,36] used the National Instruments data acquisition system for reading the position and completing the force feedback. This system was a success and showed improvements in the operational efficiency but it had its own disadvantages as it introduced significant amount of phase-lag between force-feedback and displacement into the system. The phase lag was mainly because of the data acquisition system where the analog to digital conversion (ADC) and digital to analog conversion (DAC) should run through a digital filter

before performing. The phase-lag was clocked between 9 ms, which was not acceptable for FIM measurements or energy harnessing. The phase-lag was compensated by introducing four dynamic terms with memory to model the hysteresis effects [33].

In the current research, a controller embedded virtual spring–damping system (V_{ck}) for FIM experiments is developed for each oscillator. Each oscillator consists of one interchangeable cylinder, which is designed to reduce the static/dynamic friction, has adjustable mass, and moves on submerged roller blocks. The mechanical part of the oscillator is being simulated by the controller providing the feedback through belts and pulleys. An Arduino embedded board controls the servomotor, which has an optical encoder. Digital signal is chosen, making the system more responsive, theoretically with no lag expect for that due to the central processing unit operation clocked to 10 μs. This approach enables real-time position/speed measurement.

2.2 Physical V_{ck} VIVACE System. By introducing passive turbulent control (PTC), the MRELab research team was able to reduce VIV [37,38] and at the same time to initiate galloping, and to achieve back-to-back VIV and galloping on a single circular cylinder [39]. The effects of PTC on multicylinder FIM were further studied experimentally by Kim et al. [11] and using CFD by Ding et al. [40,41]. In Kim's study, the oscillatory amplitudes of the multiple cylinders reached the limitation of the facility at flow speed of 1.5 m/s, which is below the maximum flow speed of the water channel. In 2011, in order to investigate further the FIM of cylinders with fewer restrictions, both the channel and the new VIVACE converter were rebuilt. This third generation of test-models was designed and built as shown in Figs. 1–4. In the new design, the linear motion mechanism was brought under water, which resulted in most of the structural elements being under water. The whole linear motion system, which consists of a sliding block, timing belt, and pulleys, is fitted inside of a 1.5 in. wide slender tube. The sliding block connects the cylinder to the V_{ck} system through the timing belts and pulleys as shown in Fig. 2. The mass ratio can be changed by putting a mass-shaft inside the cylinder, as shown in Fig. 3. There is a shock absorber to protect the cylinder from hitting the plexi-glass at the bottom of the water channel. The center-to-center distance (d/D) between the cylinders in the flow direction can be adjusted by the rail system starting at 5 in. and increased by 0.5 in. The features of the new VIVACE converter are summarized in Table 1.

2.3 Math Model for a V_{ck} VIVACE System. The physical model (Fig. 5) is assumed to have structural symmetry and the gravitational force is balance by spring pretension. Thus, the cylinder oscillates around its equilibrium position after the virtual springs and damper have been implemented. Table 2 shows the components in the V_{ck} system.

The equations of motion of the new VIVACE system with the embedded V_{ck} are Eqs. (1)–(5)

$$(J_{motor} + J_{pulley})\ddot{\theta}_1 = T_{motor} - t_{motor} + r_{pulley}(F - F_2) \tag{1}$$

$$J_{pulley}\ddot{\theta}_2 = -t_{pulley3} + r_{pulley}(F_1 - F_2) - 2t_{pulley2} \tag{2}$$

$$J_{pulley}\ddot{\theta}_3 = 2t_{pulley2} + r_{pulley}(F_3 - F_5) - t_{pulley3} \tag{3}$$

$$J_{pulley}\ddot{\theta}_4 = -t_{pulley1} + r_{pulley}(F_5 - F_4) \tag{4}$$

$$M_{OSC}\ddot{y} = -f_{bearing} + 2(F_4 - F_3) \tag{5}$$

Assuming that the timing-belts are inelastic, the kinematic relations among θ_i and y are:

$$\theta_1 = \theta_2 = \theta_3 = \theta \tag{6}$$

$$y = r_{pulley}\theta \tag{7}$$

Thus, Eqs. (1)–(5) are simplified to Eq. (8), by utilizing Eqs. (6) and (7)

$$\begin{aligned}(J_{motor} + 6J_{pulley} + M_{osc}r_{pulley}^2)\ddot{\theta} &= T_{motor} - t_{motor} \\ &-6t_{pulley2} - 3t_{pulley2} - 3t_{pulley3} - 2t_{pylley1} - f_{bearing}r_{pulley}\end{aligned} \tag{8.1}$$

$$\begin{aligned}(J_{motor} + 6J_{pulley} + M_{osc}r_{pulley}^2)\ddot{\theta} &= T_{motor} \\ &-(t_{motor} + 2t_{pylley} + 6t_{pulley2} + 3t_{pulley3} + f_{bearing}r_{pulley})\end{aligned} \tag{8.2}$$

$$\begin{aligned}\left(\frac{J_{motor}}{r_{pulley}^2} + \frac{6J_{pulley}}{r_{pulley}^2} + M_{OSC}\right)\ddot{y} &= \frac{T_{motor}}{r_{pulley}} \\ &-\left(\frac{t_{motor}}{r_{pulley}} + \frac{2t_{pulley}}{r_{pulley}} + \frac{6t_{pulley2}}{r_{pulley}} + \frac{3t_{pulley3}}{r_{pulley}} + f_{bearing}\right)\end{aligned} \tag{8.3}$$

Assuming that $F_{motor} = T_{motor}/r_{pulley}$, the above equation can be simplified for convenience as

$$m\ddot{y} = F_{motor} - f \tag{9}$$

where

$$m = \frac{J_{motor}}{r_{pulley}^2} + \frac{6J_{pulley}}{r_{pulley}^2} + M_{OSC} \tag{10}$$

$$f = \frac{t_{motor}}{r_{pulley}} + \frac{2t_{pulley}}{r_{pulley}} + \frac{6t_{pulley2}}{r_{pulley}} + \frac{3t_{pulley3}}{r_{pulley}} + f_{bearing} \tag{11}$$

3 SI for V_{ck}

In this application, NI-7340 samples data and is clocked at 1000 Hz compared to previous V_{ck} 200 Hz. The servodrive QS1A05AA is connected to the Arduino Due (ARM® Cortex®-M3, 32-bit ARM Cortex M3 Process clocked at 84 MHz) board through Universal Motion Interface UMI-7764. The servodrive operates in torque-command mode and receives via the servomotor in order to produce motion proportional to the command signal. The control scheme for V_{ck} is shown in Fig. 6.

3.1 Calibration of Virtual Spring. As shown in Fig. 7, in order to calibrate the torque of motor (T_{motor}) and voltage output (V_{out}), different weights (thus torque) are added to capture the referenced voltage. The calibration results are shown in Fig. 8. The calibration formula derived is

$$T_{motor} = 4.965V_{out} \tag{12}$$

With the current physical system, by considering the pulleys, the force applied to the system can also be plotted as in Fig. 9.

Based on the motor torque versus voltage calibration, variable spring constants are defined. Due to test-bed limitations, the last five spring constants only used three weights. Weights applied to the system are shown in Table 3. In Fig. 10, tick-marks are experimental k values, and solid lines are calculated k values.

The result shows congruent linear relation between the defined virtual spring constant and the output spring function. The forces tested are sufficient for the FIM experiment. Thus, the virtual spring constant values are sufficient for the experiments.

Repeatability of the virtual spring was validated by adding weights and measuring the resulting displacement. Figure 11 shows the relation between displacement and weight for $k = 800$.

3.2 Virtual, Nonlinear, Viscous Damping Model. The main function of the V_{ck} system is to add linear adjustable damping to the system to harness MHK energy. To develop the sought power

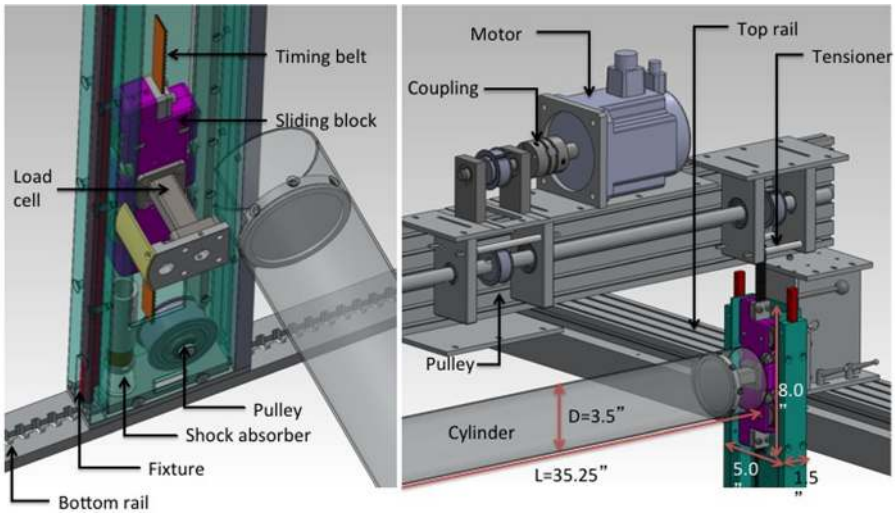

Fig. 2 Details of the new VIVACE converter

Fig. 3 Details of the cylinder design

envelope, systematic tests need to be conducted. Prior to adding prescribed damping, the physical system damping needs to be identified and subtracted. The latter is due to all moving parts, especially the timing belts and pulleys which bring undesirable/excessive amount of nonlinear damping to V_{ck}. The mechanical equation of the V_{ck} system can be expressed as

$$m\ddot{y} + c(\dot{y}) + ky = F_{\text{total}} \tag{13}$$

where F_{total} is the total hydrodynamic transverse force acting on the cylinder. So the damping model can be obtained through

$$c(\dot{y}) = F_{\text{total}} - m\ddot{y} - ky \tag{14}$$

In order to find the nonlinear viscous damping and static friction, the total damping force f, which contains motor, pulleys, and bearings, can be expressed as

$$f = f_{\text{motor}} + f_{\text{pulley}} + f_{\text{bearing}} \tag{15}$$

which can also be expressed as a function of dy/dt. Here, all the damping force is assumed to be the sum of nonlinear viscous damping of a third-order polynomial friction

$$c(\dot{y}) = c_3\dot{y}^3 + c_2\dot{y}^2 + c_1\dot{y} + c_c\text{sign}(\dot{y}) \tag{16}$$

c_1, c_2, and c_3 are the first-, second-, and third-order coefficients, respectively, and c_c, is the coulomb friction coefficient.

Fig. 4 (*a*) Two new VIVACE converters mounted in the LTFSW channel and (*b*) one VIVACE converter with V_{ck} mounted in the LTFSW channel

Table 1 Specifications of the new VIVACE converter

Mass ratio	Aspect ratio	Maximum oscillatory amplitude	Longitudinal distance
$0.634 \le m^* \le 2.00$	$L/D = 10.07$	$A_{\max}/D_{3.5''} = 5.5$	$1.429 \le d/D_{3.5''} \le 6.0$

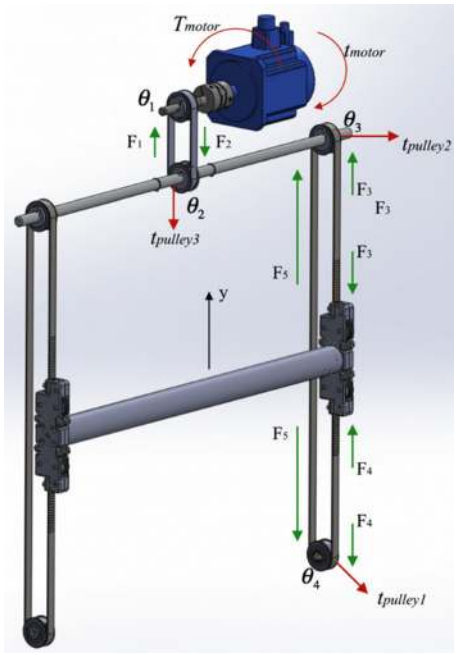

Fig. 5 Symmetric V_{ck} model with notation

Table 2 Components of embedded V_{ck} system

$\theta_i, i = 1, 2, 3, 4$	$i = 1$: angle of the motor coupling and pulley $i = 2$: angle of the pulley top-center $i = 3$: angle of the pulley top-right $i = 4$: angle of the pulley lower-right
Y	Displacement of the cylinder
M_{osc} (kg)	Equivalent mass of oscillating components
J_{motor} (kg/m^2)	Mass moment of inertia of the motor
t_{motor} (N)	Nonlinear damping torque of the motor
T_{motor} (NM)	Torque generated by the motor
J_{pulley} (kg/m^2)	Mass moment of inertia of the pulley
$t_{pulley,i}$ $i = 1, 2, 3, 4$	Nonlinear damping torque of ith pulley
r_{pulley} (m)	Radius of all pulleys
$f_{bearing}$ (N)	Nonlinear damping force of all bearings
F_i (N)	ith tension of the time-belt

The first generation of V_{ck} system [33] had a closed-loop of the vibration components and the cylinder could be detached from the belt. Constant forces were applied continuously to the timing belt to achieve sufficient speed. The new V_{ck} system has sliding blocks and timing belts inside the structure and, thus, they cannot be disconnected (Fig. 5). To achieve sufficient speed and acceleration, various single direction forces are fed to the system by the motor. Programed stoppers are set when the cylinder reaches the upper and lower ends of the travel to prevent collisions with the plexiglass bottom of the LTFSW Channel.

Figure 12 shows the experimental and curve fitting results. Table 4 shows the speed, acceleration, and associated applied forces. The regression curves are shown in the following equations:

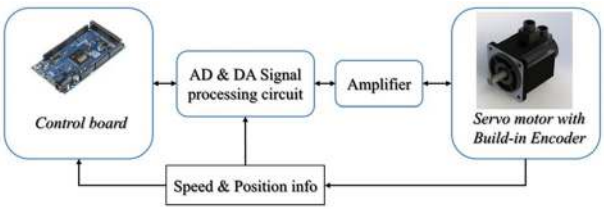

Fig. 6 Calibration of spring stiffness k for the V_{ck} system

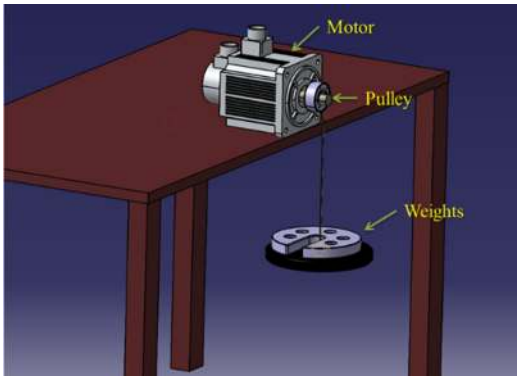

Fig. 7 V_{ck} torque calibration for k

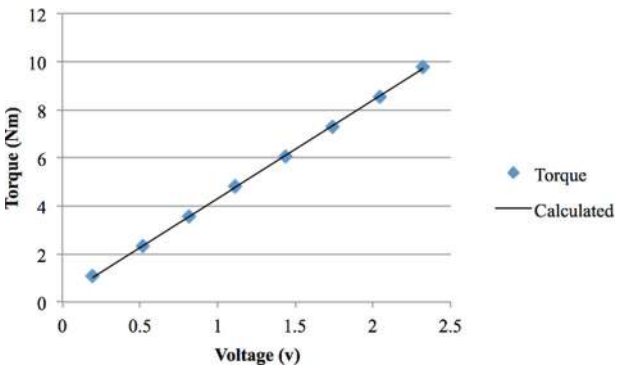

Fig. 8 Torque versus voltage from controller

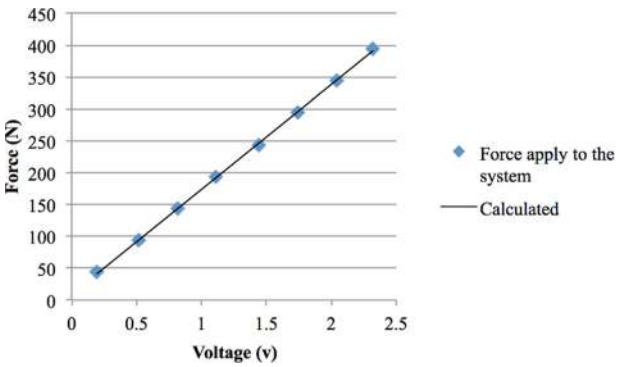

Fig. 9 Force versus voltage from controller to oscillator

$$c(\dot{y}) = 0.8793\dot{y}^3 - 7.7678\dot{y}^2 + 23.736\dot{y} + 13.439, \text{ when } \dot{y} > 0 \quad (17)$$

$$c(\dot{y}) = 1.1544\dot{y}^3 + 9.2064\dot{y}^2 + 25.992\dot{y} - 12.434, \text{ when } \dot{y} < 0 \quad (18)$$

The sinusoidal forces were fed to the system in which the damping force was calculated as

Table 3 Weight applied to the system

	1	2	3	4
Weights added (N)	44.492	89.327	134.75	179.242

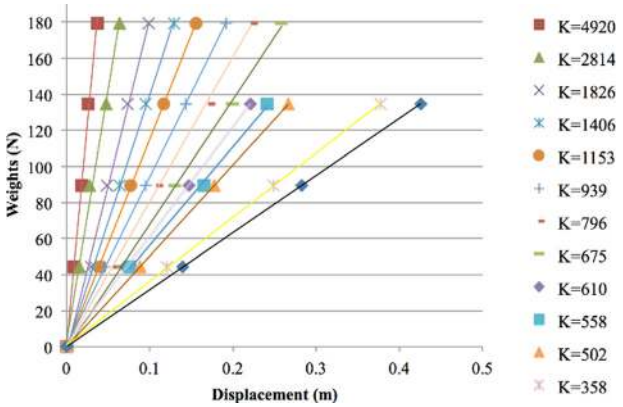

Fig. 10 Control experimental result for spring constants

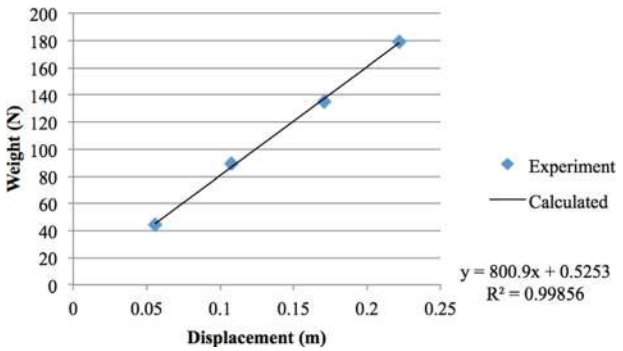

Fig. 11 Virtual spring setting test curve fitting

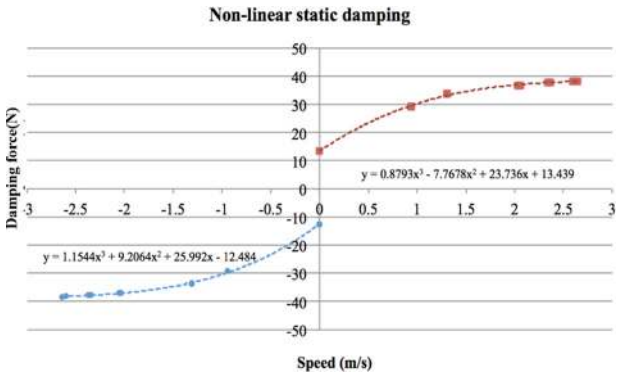

Fig. 12 NS damping map

Table 4 Identification of nonlinear viscous damping plus kinetic friction model

Velocity $\dot{y} > 0$			Velocity $\dot{y} > 0$		
$\dot{y}$ (m/s)	Force (N)	$\ddot{y}$ (m^2/s)	$\dot{y}$ (m/s)	Force (N)	$\ddot{y}$ (m^2/s)
0.933	29.28	0.618	−0.940	−28.281	0.628
1.299	33.64	1.451	−1.303	−32.606	1.551
1. 289	33. 824	1.451	−1.306	−32.606	1.651
2. 303	36.815	4.131	−2.030	−35.93	4.331
2.131	36.726	4.148	−2.055	−35.727	4.248
2.11	37. 297	5.590	−2.337	−36.433	5.6
2.367	37. 654	5.597	−2.370	−37.222	5.7
2.59	38.133	7.151	−2.59	−38.153	7.351
2.65	38.208	7.147	−2.642	−39.294	7.447
0	13.506	0	0	−12.506	0

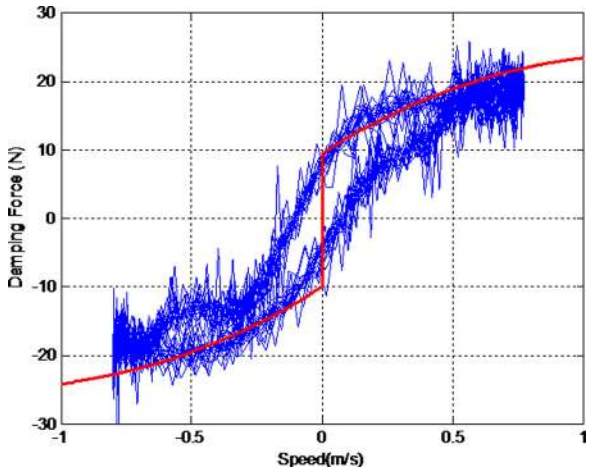

Fig. 13 Force amplitude 75 N, frequency 0.8 Hz

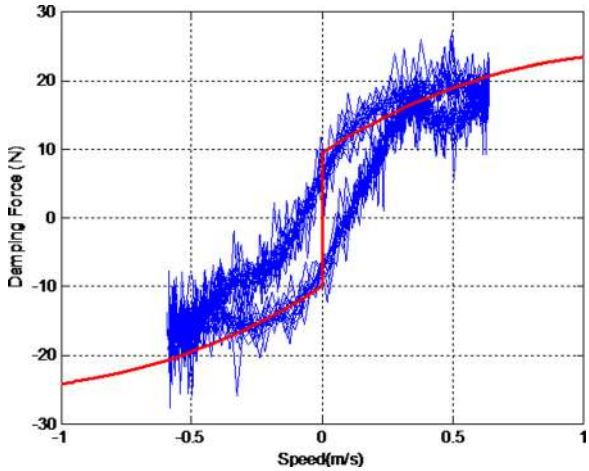

Fig. 14 Force amplitude 60 N, frequency 0.8 Hz

$$c(\dot{y}) = F\sin(\omega t + \varphi) - m\ddot{y} - ky \tag{19}$$

where F is force amplitude. A low pass filter was applied to attenuate the noise caused by numerical differentiation. Figures 13–15 show the damping force versus the nonlinear static (NS) model. The blue line is the damping force, and the red line is the NS model applied by the controller. All the spring constants were set to be 600 N/m.

3.3 Controller Design. Based on the nonlinear viscous damping model, the controller force can be expressed as

$$F_{\text{controller}} = F_{\text{fluid}} - c_{\text{virtual}}\dot{y} - k_{\text{virtual}}y \tag{20}$$

where $F_{\text{controller}}$ is the force applied by the virtual system, F_{fluid} is the total hydrodynamic force acting on the cylinder, k_{virtual} is the virtual spring constant, c_{virtual} is the virtual linear viscous damping. c_{virtual} is added after subtracting the nonlinear viscous damping defined by Eqs. (17) and (18).

Free decay tests are also performed to verify the subtraction of the system damping and the application of the linear viscous damping. The spring constants were set to 600 N/m and 800 N/m, respectively. All experiments were performed with gradually increasing the linear viscous damping from 10% to 90% of the system, Fig. 16, Table 5, and Table 6 show the free decay test results. The repeatability was checked five times for each spring constant. Where c is the damping of the system, m^* is the mass ratio, Td is the oscillation period, and ω_n is natural frequency of the system in vacuum.

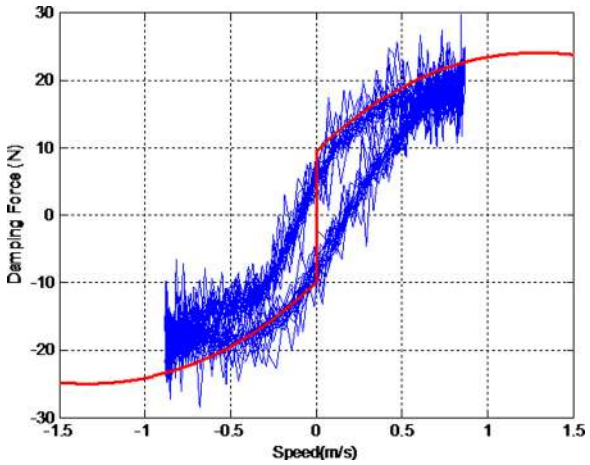

Fig. 15 Force amplitude 60 N, frequency 1.0 Hz

4 Controlled FIM Experiments

Experiments were first designed and performed covering the entire range of VIV and galloping to verify the effectiveness of the V_{ck} system. A real spring was used instead of the V_{ck} and timing belts. Since the inertial mass of VIVACE with V_{ck} is larger than one-third of the real spring mass, additional mass was put inside the oscillator to match the mass ratio of V_{ck} and the physical springs system. Free decay experiments were performed to measure the damping.

Figure 17 shows comparison of amplitude ratio A/D between tests with real springs and with the V_{ck} VIVACE model. The range of velocities covers VIV and galloping until the facility limit is reached. Error bars are shown in the form of one standard deviation. The reduced velocity U^* is

$$U^* = \frac{U}{f_n D} \tag{21}$$

where U is the flow speed, f_n is the natural frequency in water

$$f_n = \frac{1}{2\pi}\sqrt{\frac{k}{m+m_a}} \tag{22}$$

and m_a is added mass. Discussion of modeling of m_a can be found in Ref. [33].

The agreement between the real spring system and V_{ck} is very good in VIV and galloping measurements over the entire range of velocities tested. The V_{ck} system tends to initiate galloping sooner

Table 5 Free decay results for $k_{virtual}$ = 600 N/m

k (N/m)	Damping ratio	c (Ns/m)	m_{osc} (kg)	m^*	T_d	ω_n
600	0.0537	6.15	5.4555	1.006	0.6	10.487
600	0.0453	5.204	5.4874	1.012	0.6015	10.457
600	0.0355	4.056	5.4508	1.005	0.6	10.492
600	0.0276	3.161	5.4581	1.006	0.601	10.485
600	0.0216	2.469	5.4597	1.006	0.602	10.483
600	0.0146	1.679	5.4747	1.009	0.603	10.469
Stand dev.			0.013863	0.00265	0.001172	0.01318

Table 6 Free decay results for $k_{virtual}$ = 800 N/m

K (N/m)	Damping ratio	C (N s/m)	m_{osc} (kg)	m^*	T_d	ω_n
800	0.689	9.222	5.6066	1.033	0.5273	11.945
800	0.593	7.939	5.5975	1.032	0.5265	11.955
800	0.0511	6.837	5.592	1.031	0.5255	11.961
800	0.0459	6.15	5.6028	1.033	0.527	11.949
800	0.0349	4.673	5.6131	1.035	0.527	11.938
800	0.0216	3.501	5.6241	1.037	0.527	11.927
800	0.0178	2.391	5.6155	1.035	0.5245	11.936
Stand dev.			0.0121	0.00222	0.00103	0.0128

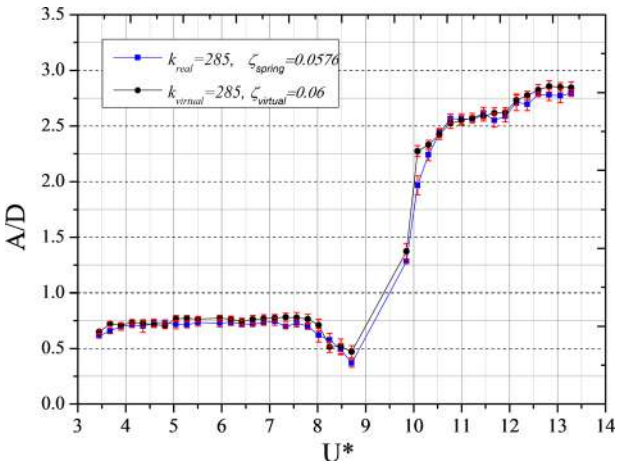

Fig. 17 Control PTC (passive turbulence control: 20–36 deg) experiment for real and V_{ck} system at m^* = 1.658

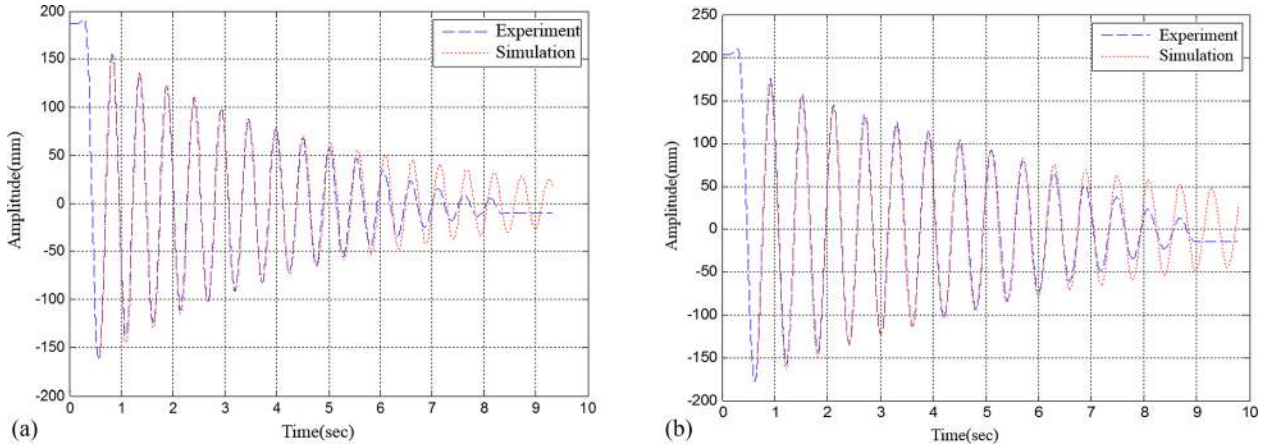

Fig. 16 Free decay tests for V_{ck} at $k_{virtual}$ = 600 and 800 N/m

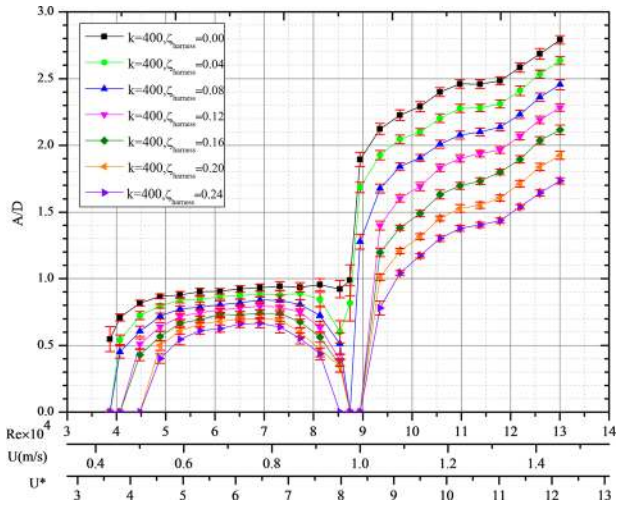

Fig. 18 Amplitude ratio versus Re, *U*, *U** for $k = 400$ N/m and various values of ζ_{hamess}

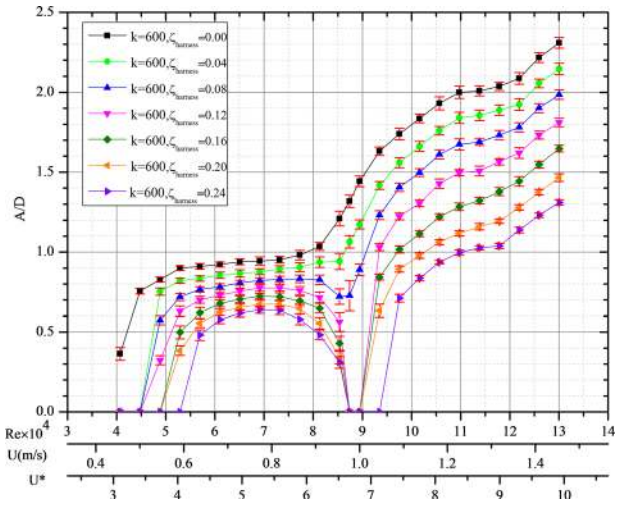

Fig. 21 Amplitude ratio versus Re, *U*, *U** for $k = 600$ N/m and various values of ζ_{hamess}

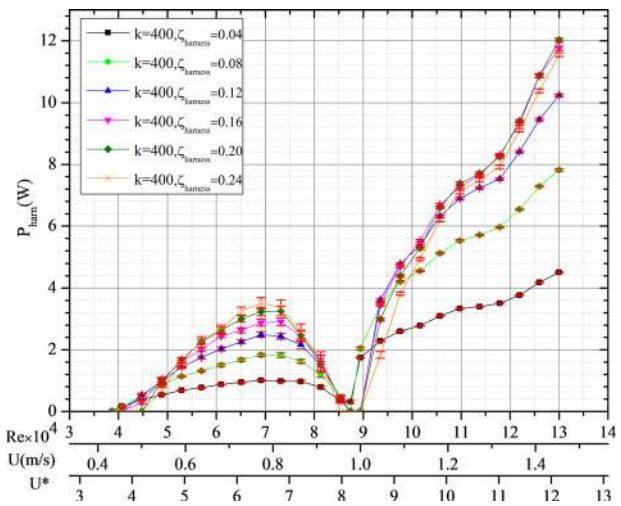

Fig. 19 Harness power for $k = 400$ N/m; various values of ζ_{hamess}

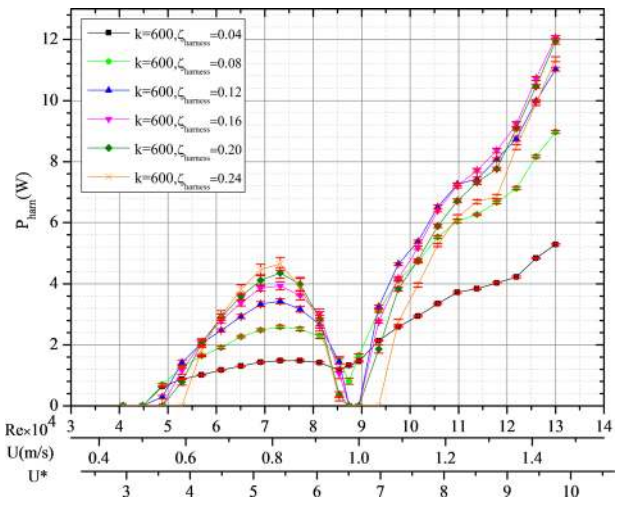

Fig. 22 Harness power for $k = 600$ N/m; various values of ζ_{hamess}

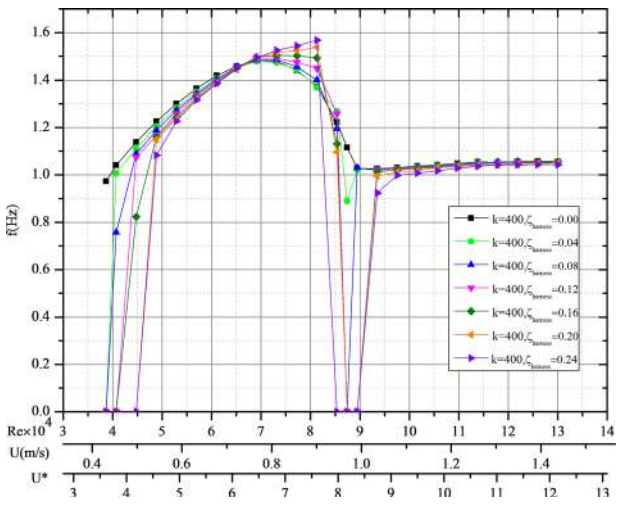

Fig. 20 Vibration frequency in water for $k = 400$ N/m and various values of ζ_{hamess}

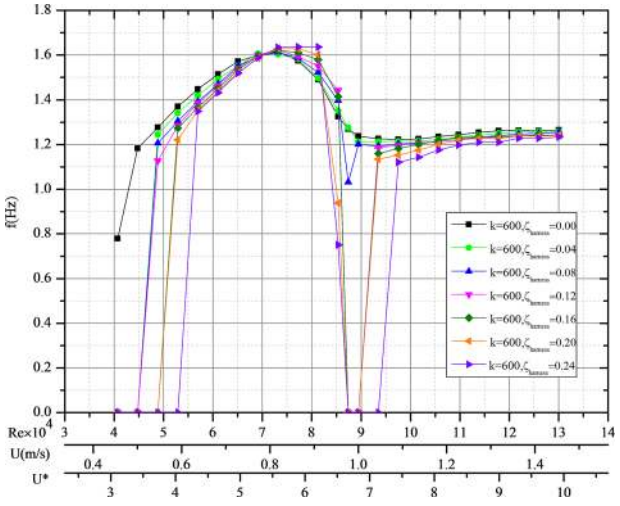

Fig. 23 Vibration frequency in water for $k = 600$ N/m and various values of ζ_{hamess}

than the real spring experiment at the reduced velocity around ten. That is the transition region from VIV to galloping. That can be attributed to additional drag force caused by the spring vibration, which can create slight added turbulence during FIM.

Typical results of FIM experiments performed by V_{ck} are shown in Figs. 18–23. They show A/D, the average harnessed power, and frequency of oscillation by processing data over 30 cycles away from transients. The points exhibiting the zero oscillation frequency indicate that the cylinder FIM stops due to high damping. Extensive experiments for different mass ratio will be performed for harness energy in the near future. The spring stiffness $k = 400$ N/m for Figs. 18–20 and 600 N/m for Figs. 21–23.

5 Conclusions

An embedded virtual spring–damping system V_{ck}, designed for FIM experiments, was developed, verified, and validated in this research by extensive calibration and comparison to physical spring–damper oscillators. In the V_{ck}, the spring and damping constants are programmable. The torque simulating the mechanical part of the oscillator is provided by a servomotor driven by a controller. The hydrodynamic force is not affected, as it is not included in the control loop.

In the new VIVACE oscillators, most of the structural components including the linear motion mechanism consisting of a sliding block, timing belts, and pulleys were brought under water. The new system better models the field-deployed devices compared to previous models. A resistor bank is used to dissipate the generated power.

The SI process was developed for the oscillator that can also be extended to any electrically based single degree-of-freedom oscillator. Upon subtracting the identified nonlinear damping model using the controller, a mathematically linear damping model was added, which results in a system with adjustable, ideally linear, viscous damping. This process enables changing the spring constant k and harnessing damping $c_{harness}$ through the controller instantly.

The main improvement of the new V_{ck} system is that it was developed as a standalone application via an embedded controller. Digital signals are used compared to analog signals in the earlier version of V_{ck}. The sample time was reduced by three orders of magnitude, thus, eliminating the need to include dynamic terms with memory in the damping model to achieve no bias in FIM and energy harnessing. Compensating for the system nonlinear damping makes it possible to introduce a theoretically linear viscous damping, which can hardly be achieved in engineering applications; and yet is used in modeling oscillators.

Control experiments were performed to verify the effectiveness of the virtual system using the spring constant of 400 N/m and 600 N/m. The agreement between physical and virtual springs and dampers was excellent in FIM measurements over the entire range of spring constants and velocities tested.

Tests were performed for FIM measurements and energy harnessing for $0.00 < \zeta_{harness} < 0.24$. The embedded V_{ck} system enables systematic experiments with different mass ratios, variable k and $c_{harness}$, and multiple oscillators needed to generate envelopes for the VIVACE converter.

Acknowledgment

The following supports are gratefully acknowledged: DOE Contract No. DE-EE0006780 to Vortex Hydro Energy with subcontract to the University of Michigan; Ministry of Industry and Information Technology of the P. R. China, Project No. G014614002.

References

[1] Bearman, P. W., 1984, "Vortex Shedding From Oscillating Bluff Bodies," Annu. Rev. Fluid Mech., **16**(1), pp. 195–222.
[2] Bearman, P. W., 2011, "Circular Cylinder Wakes and Vortex-Induced Vibrations," J. Fluid Mech., **27**, pp. 648–658.
[3] Sarpkaya, T., 2004, "A Critical Review of the Intrinsic Nature of Vortex-Induced Vibrations," J. Fluids Struct., **19**(4), pp. 389–447.
[4] Williamson, C. H. K., and Govardhan, R., 2004, "Vortex-Induced Vibrations," Annu. Rev. Fluid Mech., **36**, pp. 413–455.
[5] Blevins, R. D., and Coughran, C. S., 2009, "Experimental Investigation of Vortex-Induced Vibration in One and Two Dimensions With Variable Mass, Damping, and Reynolds Number," ASME J. Fluids Eng., **131**(10), p. 101202.
[6] Alonso, G., Meseguer, J., and Pérez-Grande, I., 2005, "Galloping Instabilities of Two-Dimensional Triangular Cross-Section Bodies," J. Exp. Fluids, **38**(6), pp. 789–795.
[7] Zdravkovich, M. M., 1997, *Flow Around Circular Cylinders*, Vol. 1, E. Achenbach, ed., Oxford University Press, Oxford.
[8] Bernitsas, M. M., Simon, Y. B., Raghavan, K., and Garcia, E. M. H., 2009, "The VIVACE Converter: Model Tests at High Damping and Reynolds Number Around 10^5," ASME J. Offshore Mech. Arct. Eng., **131**(1), p. 011102.
[9] Raghavan, K., and Bernitsas, M. M., 2011, "Experimental Investigation of Reynolds Number Effect on Vortex Induced Vibration of Rigid Cylinder on Elastic Supports," J. Ocean Eng., **38**(5), pp. 719–731.
[10] Chang, C. C., Kumar, R. A., and Bernitsas, M. M., 2011, "VIV and Galloping of Single Circular Cylinder With Surface Roughness at $3.0 \times 10^4 \leq \mathrm{Re} \leq 1.2 \times 10^5$," J. Ocean Eng., **38**(16), pp. 1713–1732.
[11] Kim, E. S., Bernitsas, M. M., and Kumar, A. R., 2011, "Multi-Cylinder Flow Induced Motions: Enhancement by Passive Turbulence Control at $28{,}000 < \mathrm{Re} < 120{,}000$," ASME, J. Offshore Mech. Arct. Eng., **135**(1), p. 021802.
[12] Kim, E. S., 2013, "Synergy of Multiple Cylinders in Flow Induced Motion (FIM) for Hydrokinetic Energy Harnessing," Ph.D. thesis, The University of Michigan, Ann Arbor, MI.
[13] Zdravkovich, M. M., 2002, *Flow Around Circular Cylinders*, Vol. 2, E. Achenbach, ed., Oxford University Press, Oxford.
[14] Chen, S. S., 1986, "A Review of Flow Induced Vibration of Two Circular Cylinders in Crossflow," ASME J. Pressure Vessel Technol., **108**(4), pp. 382–393.
[15] Zdravkovich, M. M., 1988, "Review of Interference Induced Oscillations in Flow Past Two Parallel Circular Cylinders in Various Arrangements," J. Wind Eng. Ind. Aerodyn., **28**(1–3), pp. 183–200.
[16] Zdravkovich, M. M., and Medeiros, E. B., 1991, "Effect of Damping on Interference-Induced Oscillations of Two Identical Circular Cylinders," J. Wind Eng. Ind. Aerodyn., **38**(2–3), pp. 197–211.
[17] Bernitsas, M. M., and Raghavan, K., 2009, "Fluid Motion Energy Converter," United States Patent and Trademark Office, Patent No. 7,493,759 B2.
[18] Bernitsas, M. M., and Raghavan, K., 2011, "Enhancement of Vortex Induced Forces and Motion Through Surface Roughness Control," U.S. Patent Trademark Office, Patent No. 8,042,232 B2.
[19] Bernitsas, M. M., and Raghavan, K., 2014, "Reduction of Vortex Induced Forces & Motion Through Surface Roughness Control," U.S. Patent and Trademark Office, Patent No. 8,684,040 B2.
[20] Bernitsas, M. M., and Raghavan, K., 2007, "Reduction/Suppression of Vortex Induced Forces and Motion Through Surface Roughness Control," U.S. Provisional Patent Application No. US2009/0114002 A1 (UofM#3757).
[21] Chang, C. C., and Bernitsas, M. M., 2011, "Hydrokinetic Energy Harnessing Using the VIVACE Converter With Passive Turbulence Control," ASME Paper No. OMAE2011-50290.
[22] Raghavan, K., 2007, "Energy Extraction From a Steady Flow Using Vortex Induced Vibration," Ph.D. thesis, The University of Michigan, Ann Arbor, MI.
[23] Garcia, M. H. E., 2008, "Vortex Coalescence in Vortex Induced Vibrations for Ocean Energy Harness," Ph.D. thesis, The University of Michigan, Ann Arbor, MI.
[24] Chang, C. C., 2010, "Passive Turbulence Control for VIV Enhancement for Hydrokinetic Energy Harnessing Using Vortex Induced Vibrations," Ph.D. thesis, The University of Michigan, Ann Arbor, MI.
[25] Wu, W., 2011, "CFD Modeling and Model-Test Calibration of VIV of Cylinders With Surface Roughnessm," Ph.D. thesis, The University of Michigan, Ann Arbor, MI.
[26] Lee, J. H., 2010, "Hydrokinetic Power Harnessing Utilizing Vortex Induced Vibrations Through a Virtual c–k VIVACE Model," Ph.D. thesis, The University of Michigan, Ann Arbor, MI.
[27] Park, H. R., 2012, "Mapping of Passive Turbulence Control to Flow Induced Motions of Circular Cylinders," Ph.D. thesis, The University of Michigan, Ann Arbor, MI.
[28] Zhu, H., Aiman Al-Showaiter, A., Ayman Eltaher, A., Whooley, A., and Jukes, P., 2012, "Cross Flow VIV Analysis of a Subsea Pipeline and Jumper Using FSI Method," Society of Petroleum Engineers Annual Technical Conference and Exhibition, San Antonio, TX, Oct. 8–10.
[29] Meliga, P., and Chomaz, J., 2011, "An Asymptotic Expansion for the Vortex-Induced Vibrations of a Circular Cylinder," J. Fluid Mech., **671**, pp. 137–167.
[30] Barrero-Gil, A., Pindado, S., and Avila, S., 2012, "Extracting Energy From Vortex-Induced Vibrations: A Parametric Study," Appl. Math. Model., **36**(7), pp. 3153–3160.
[31] Konstantinidis, E., 2013, "Apparent and Effective Drag for Circular Cylinders Oscillating Transverse to a Free Stream," J. Fluids Struct., **39**, pp. 418–426.
[32] Kang, Z., and Jia, L. S., 2013, "An Experimental Investigation of One-and Two-Degree Of Freedom VIV of Cylinders," Acta Mech. Sin., **29**(2), pp. 284–293.
[33] Lee, J. H., Xiros, N., and Bernitsas, M. M., 2011, "Virtual Damper–Spring System for VIV Experiments and Hydrokinetic Energy Conversion," J. Ocean Eng., **38**(5), pp. 732–747.

[34] Smogeli, Ø. N., Hover, F. S., and Triantafyllou, M. S., 2003, "Force-Feedback Control in VIV Experiments," ASME Paper No. OMAE2003-37340.
[35] Mackowski, A. W., and Williamson, C. H. K., 2011, "Developing a Cyber-Physical Fluid Dynamics Facility for Fluid-Structure Interaction Studies," J. Fluids Struct., **27**(5–6), pp. 748–757.
[36] Lee, J. H., and Bernitsas, M. M., 2011, "High-Damping, High-Reynolds VIV Tests for Energy Harnessing Using the VIVACE Converter," J. Ocean Eng., **38**(16), pp. 1697–1712.
[37] Park, H. R., Bernitsas, M. M., and Kumar, R. A., 2012, "Selective Roughness in the Boundary Layer to Suppress Flow-Induced Motions of Circular Cylinder at $30{,}000 < \mathrm{Re} < 120{,}000$," ASME J. Offshore Mech. Arct. Eng., **134**(4), p. 041801.
[38] Park, H. R., Bernitsas, M. M., and Kim, E. S., 2014, "Selective Surface Roughness to Suppress Flow-Induced Motions of Two Circular Cylinders at $30{,}000 < \mathrm{Re} < 120{,}000$," ASME J. Offshore Mech. Arct. Eng., **136**(4), p. 041804.
[39] Wu, W., Bernitsas, M. M., and Maki, K., 2011, "RANS Simulation vs. Experiments of Flow Induced Motion of Circular Cylinder With Passive Turbulence Control at $35{,}000 < \mathrm{Re} < 130{,}000$," ASME Paper No. OMAE2011-50311.
[40] Ding, L., Bernitsas, M. M., and Kim, E. S., 2013, "2-D URANS Versus Experiments of Flow Induced Motions of Two Circular Cylinders in Tandem With Passive Turbulence Control for $30{,}000 < \mathrm{Re} < 105{,}000$," J. Ocean Eng., **72**, pp. 429–440.
[41] Ding, L., Zhang, L., Kim, E. S., and Bernitsas, M. M., 2015, "URANA Versus Experiments of Flow Induced Motions of Multiple Circular Cylinder With Passive Turbulence Control," J. Fluids Struct., **54**, pp. 612–628.